Earthquake growth inhibited at higher Coulomb stress change rate at Groningen.

Y. Tamama[1], M. Acosta[1], S. J. Bourne[2], and J. P. Avouac[1]

[1]Department of Geological and Planetary Sciences, California Institute of Technology, Pasadena, CA, USA
[2]Shell Global Solutions International B.V., Amsterdam, The Netherlands

Key Points:

- We report a positive correlation between the Gutenberg-Richter b-value and the rate of Coulomb stress change of induced earthquakes in Groningen.
- This trend is statistically significant and robust to changes in the mechanical model used to calculate the stress changes.
- We interpret earthquake growth inhibition through a decrease of nucleation lengths at high stress change rates.

Corresponding author: Yuri Tamama, `ytamama@caltech.edu`

Abstract

Gas extraction from the Groningen gas field resulted in significant induced seismicity. We analyze the magnitude-frequency distribution of these earthquakes in space, time and in view of stress changes calculated based on gas production and reservoir properties. Previous studies suggested variations related to reservoir geometry and stress. While we confirm the spatial variations, we do not detect a clear sensitivity of b-value to Coulomb stress changes. However, we find that b-value correlates positively with the rate of Coulomb stress changes. This correlation is statistically significant and robust to uncertainties related to stress calculation. This study thus points to a possible influence of stress change rate on the magnitude probability of induced earthquakes.

Plain Language Summary

Gas extraction from an underground reservoir in the Netherlands has induced significant seismicity. We analyse how stress changes and the rate of stress changes influence the magnitude of these earthquakes. We find that more smaller earthquakes tend to occur at higher stress change rates. Earthquakes triggered at a lower stress change rate may thus grow to larger magnitudes than those triggered at high stress change rate. This observation is statistically significant and independent of the method used to calculate stress change.

1 Introduction

The factors influencing earthquake magnitude is a subject of active research. While fault geometry (Stirling et al., 1996; T. H. Goebel et al., 2017) plays a role, it is commonly admitted that higher stresses promote larger magnitudes (Scholz, 1968, 2015; Schorlemmer et al., 2005; Rivière et al., 2018). The effect seems visible in examples of injection-induced seismicity (Mukuhira et al., 2021, 2024) and seismicity induced by gas extraction at Groningen (Bourne & Oates, 2020; Kraaijpoel et al., 2022; Muntendam-Bos & Grobbe, 2022). Here, we reanalyze the case of Groningen (Fig. 1a, b). The motivation for this reanalysis is that previous studies have only considered annually averaged stress changes, while in reality gas production is highly seasonal (Fig. S1). We use a geomechanical model calibrated with measurements of surface deformation to calculate stress changes within and outside the reservoir with subannual resolution (Meyer et al., 2023; Acosta et al., 2023) (Fig. S1). Hereafter, we present the setting and review previous studies of induced seismicity at Groningen. We then present our data and methodology and discuss our results.

2 Overview of previous studies of induced seismicity at Groningen

The Groningen gas reservoir (Fig. 1) consists of a Permian porous (∼20%) sandstone at a depth of 3 km (de Jager & Visser, 2017; Bourne et al., 2014). Reservoir thickness increases from ∼90 m to the southeast to ∼300 m in the northwest (de Jager & Visser, 2017). Earthquakes were first detected in 1991. Seismicity rate increased until 2013, and then decreased as extraction slowed (Muntendam-Bos & Grobbe, 2022) (Fig. 1d). Seismicity rate in space and time is related to reservoir compaction and can be reasonably well forecasted (Bourne & Oates, 2017; Bourne et al., 2018; Candela et al., 2019; Richter et al., 2020; Smith et al., 2022; Dempsey & Suckale, 2023; Kaveh et al., 2023). Several studies have also examined the magnitude-frequency distributions (MFD) of these earthquakes (Kaveh et al., 2023; Zöller & Hainzl, 2022; Zöller & Holschneider, 2016; Bourne et al., 2018). Estimating magnitudes is of foremost importance (Zöller & Holschneider, 2016; Bommer & van Elk, 2017), as they feed directly into risk analysis.

The MFD of earthquakes is commonly quantified using the b-value (Gutenberg & Richter, 1944). The b-value gauges the number of smaller earthquakes relative to larger ones, with high b-values indicating higher relative frequency of smaller earthquakes (Fig. 1c). In seismic hazard assessment, it is common to assume a stationary magnitude probability in time but with spatial variations. Variations in space have been identified at Groningen (Kraaijpoel et al., 2022; Gulia, 2023; Boitz et al., 2024; Muntendam-Bos & Grobbe, 2022), but other studies reveal possible variations in time. Bourne and Oates (2020) and Kraaijpoel et al. (2022) also report lower b-values at higher stresses. Their findings are consistent with observations of b-value in the laboratory (T. Goebel et al., 2013; Rivière et al., 2018) and the negative correlation between b-value and differential stress observed for natural earthquakes (Scholz, 2015).

However, three lines of evidence potentially undermine the correlation between b-value and stress at Groningen. First, the earthquakes appear to follow a spatial dependence, as opposed to a stress change dependence. For earthquakes recorded within the reservoir outline between 1991 and 2023, those associated with higher Coulomb stress changes (CSC) occupy the center of the reservoir, where there is greater compaction, while those with lower CSC occur towards the edges (Fig. 1b). While CSC follows this radial pattern, the b-values do not. Muntendam-Bos and Grobbe (2022), Gulia (2023), and Kraaijpoel et al. (2022) observe b-value increasing from the northwest to southeast, following the pattern of reservoir thickness. The second line of evidence relates to temporal resolution. Bourne and Oates (2020) and Kraaijpoel et al. (2022) use the Elastic Thin Sheet model of Bourne and Oates (2017), calculating CSC on an annual resolution. However, gas extraction and CSC follow a seasonal cycle (Acosta et al., 2023) that is not accounted in either study. Third, b-value may instead be controlled by the rate of CSC. Gulia (2023) observed a negative correlation between b-value and compaction rate, a quantity that scales with stress change rate. We are thus motivated to revisit the relationships between b-value and stress in the Groningen reservoir. To benchmark our findings with the existing literature, we also compute variations with time and space.

3 Data and methods

3.1 Data

We use the earthquake catalog of the Royal Netherlands Meteorological Institute (KNMI, 2023) and select earthquakes recorded between December 1991 and July 2023 within the reservoir outline. This catalog contains 1487 events with local magnitudes between -0.18 and 3.60. The magnitude of completeness (M_C) decreased from ∼1.50 to ∼0.50 between 1991 and 2014 as seismic monitoring improved (Dost et al., 2017; Smith et al., 2022).

3.2 Calculation of Coulomb stress change

Stress changes throughout the reservoir are calculated based on monthly pressure changes, the maximum temporal resolution of the available information on extraction data (Oates et al., 2022; Acosta et al., 2023). We first use a vertical flow equilibrium model, benchmarked with fluid pressure measurements at wells (Meyer et al., 2023), to calculate pore pressure changes in the reservoir. From pressure changes, compaction and stress changes are calculated using the geomechanical model of Smith et al. (2022) (see Text S1). The reservoir is modeled as poroelastically deforming cuboids. Each cuboid is ∼500 m in the horizontal directions and has a thickness equal to the local thickness of the reservoir. Probabilistic assessment of earthquake location by Smith et al. (2020) show that the earthquakes' depth distribution peaks just above the reservoir. We therefore sample the stress field at a depth of 5 m above the reservoir and at the center of each cuboid in the horizontal plane. We hereafter refer to this sampling scheme as the reference model. The reference model provides a good basis to predict the spatial and temporal variation of seismicity rate (Kaveh et al., 2023). To verify our results are robust to different sampling locations in our model, we test additional sampling schemes (see Table S1).

For each earthquake, we estimate the Coulomb stress change (CSC) using the normal and shear stress change calculated at the nearest time-step and sampling location. We assume a friction coefficient of 0.6 and a fault orientation optimally oriented for CSC. We also estimate the time derivative of CSC using backward differencing with the previous month. This derivative is hereafter referred to as the CSC rate. CSC rate follows a seasonal cycle, with the winters characterized by a higher rate due to greater extraction. However, CSC rate experiences a long-term decline from September 2015 (Fig. S1) due to a year-round decrease (Smith et al., 2022) and an important reduction of the seasonal swings in extraction activity (Muntendam-Bos & Grobbe, 2022). We therefore only use earthquakes occurring before September 2015, when seasonal variations are strong and probably well resolved.

3.3 Calculation of b-value

We use three methods to calculate b-value:

1. Maximum likelihood method (Aki, 1965), assuming a M_C of 1.20.
2. Modified maximum likelihood method by Kijko and Smit (2012), accounting for time-varying catalog completeness. We estimate the time-evolution of M_C from Smith et al. (2022) (see Fig. S2).
3. A method proposed by van der Elst (2021) that uses the absolute values of magnitude differences between sequential earthquakes, hereafter referred to as the "b-absolute" method. Because method is insensitive to the M_C of the catalog, the entire catalog can be used to better resolve b-value variations. We opt to use b-absolute rather than b-positive, which uses only the positive magnitude differences and therefore only half of the data. The b-positive method alleviates the fact that, during an aftershock sequence, smaller events are obscured by the temporary increase in seismic noise due to coda waves (van der Elst, 2021). In our case, the proportion of aftershocks is small, making the possible bias negligible. We verify this claim by checking that the b-positive and b-absolute methods yield values that are generally consistent (Fig. S3).

These methods differ by how they address catalog incompleteness at low magnitudes. This effect must be taken into account, as variation in the M_C with time could be a source of bias.

For an ideal earthquake catalogue following a non-truncated Gutenberg-Richter distribution, all methods should yield the same b-value within uncertainties. In practice, this might not be the case due to departures from the ideal log-linear MFD.

3.4 Variation of b-value with time, space, stress change, and stress change rate

We compute variations in b-value with time, space, CSC, and CSC rate. We group the earthquakes in overlapping bins with respect to each variable, in ascending order, and calculate the b-value of each bin. For each bin, we randomly sample, without replacement, a subset of earthquakes and calculate the b-value of each subset. We remove any earthquakes below the M_C or the magnitude differences between sequential earthquakes that are smaller than the catalog resolution. Even after sample removal, most bins and subsets end up at sizes of ∼150 and ∼100, respectively. We conduct 50 iterations of sampling, after which we calculate the median, 16th percentile, and 84th percentile of b-value across all samples. We designate the median as the b-value of that bin.

When using the modified maximum likelihood method of Kijko and Smit (2012), we divide each subset into groups of differing M_C. We calculate the b-value of each group if it contains at least 10 earthquakes. We then use the average of these b-values, weighted by the number of earthquakes per group, as the b-value of that subset.

4 Results

All three methods feature a gradient of b-value increasing from northwest to southeast (Fig. S5). These observations are consistent with Muntendam-Bos and Grobbe (2022), Gulia (2023) and Kraaijpoel et al. (2022). This gradient may be attributed to the decrease in reservoir thickness from northwest to southeast (Kraaijpoel et al., 2022), and indeed, we also uncover a negative correlation between b-value and reservoir thickness (Fig. S5d). This correlation between b-value and reservoir thickness is physically intuitive. Assuming seismogenic faults "cut through" the height of the reservoir, larger faults would exist where the reservoir is thicker, allowing for larger events and hence a lower b-value. However, the explanation for the higher b-values to the east and west is less clear.

We also find, as observed by Kaveh et al. (2023) and Gulia (2023), b-value increasing and decreasing with time (Fig. 2). This pattern roughly matches that of seismicity rate, which peaked in 2012-2015 (Fig. 1d). This faint agreement suggests that b-value might depend on the stress rate, rather than stress, as seismicity rate correlates with stress rate to the first order.

We do not see a clear variation of b-value with CSC (Fig. 2). However, when we calculate CSC using the Elastic Thin Sheet model (Bourne & Oates, 2017), updated with a monthly resolution, we recover the negative correlation between b-value and CSC observed by Bourne and Oates (2020) (Fig. 2c). This negative correlation might originate from the difference in spatial distribution between earthquakes at low and high CSC.

We do observe b-value increasing with CSC rate (Fig. 3a). From 10 Pa/day to 25 Pa/day, b-value increases from 0.6-0.8 to 0.9-1.1. Above 25 Pa/day, the b-value from the maximum likelihood methods plateaus around those values, whereas the b-value from the b-absolute method steadily declines to $\sim$0.8 (Fig. 3a).

We test whether the correlation between b-value and CSC rate is robust to the sampling locations within the mechanical model. Following Kaveh et al. (2023), we calculate CSC rate at the edge of each cuboid and at depths of 1, 10, and 50 m above the reservoir (see Table S1). We also test whether our correlation holds when using the Elastic Thin Sheet model of Bourne and Oates (2017) For all cases, we find a positive correlation between b-value and CSC rate (Fig. 3b, S6), underscoring the robustness of our observation.

5 Discussion

5.1 Statistical significance of b-value correlation with stress change rate

We assess the statistical significance of the positive correlation between b-value and CSC rate. We divide the catalog into two groups: a "low CSC rate" group below 15.7 Pa/day and a "high CSC rate" group above 15.7 Pa/day. A two-sample, two-tailed Kolmogorov–Smirnov test between these groups yields a K-S statistic of 0.078, corresponding to a p-value of 0.154. The probability that the high and low CSC rate groups originate from the same distribution is thus 15.4 percent. To evaluate the probability of having such dissimilar distributions by chance, if they are characterized by the b-value, we also conduct a jacknife test. We calculate the b-value of each group and compare these values to those calculated from random samples of half the catalog, taken without replacement. A total of 800 samples are taken. Figure 4a plots the distribution of b-values calculated from each sample, alongside b-values calculated from the high and low CSC rate groups, both of which fall on the edges of that distribution. The probability that a randomly-selected sample of earthquakes has a b-value as low as that of the low CSC rate group is 2.9 percent. Likewise, the probability for a b-value as high as that of the high CSC rate group is 1.0 percent. All b-values are calculated using the maximum likelihood method with a M_C of 1.2.

We also validate that the b-values of each group reflect their respective MFDs. Figure 4b shows the MFD of the randomly selected samples, as well as the low and high CSC rate groups. These distributions are consistent with the trend in our estimated b-values. The distribution of the high CSC rate group is steeper than that of the low CSC rate group. Furthermore, the distribution of either group falls at the edges of the distributions of the randomly selected groups. We repeat the same analyses, but for the CSC rates calculated using the Elastic Thin Sheet model (Bourne & Oates, 2017), and obtain similarly convincing results (Fig. S7).

5.2 Is the b-value an adequate metric?

We acknowledge that the b-value might not be the best quantity to characterize the MFD. Bourne and Oates (2020) argue that these distributions are better quantified using a "taper" at higher magnitudes. However, in the case of the groups with high and low CSC, the b-value is a better metric to characterize the MFD. This is evident upon visual inspection of the MFD of each group. Earthquakes at low CSC rate taper from $M =\sim 2.65$, while those at high CSC rate taper from $M =\sim 2.95$. These tapers alone, however, are insufficient to capture the difference in MFD. The high CSC rate group is characterized by larger b-values, which also reflect the steeper slope of its MFD (Fig. 4c).

We further verify the appropriateness of the b-value using K-S tests. We randomly generate 1000 synthetic catalogs obeying the Gutenberg-Richter distribution (Li et al., 2023), with b-values equal to that of the low and high CSC rate groups. We then conduct two-sample, two-tailed K-S tests between the synthetic and observed earthquakes, to assess the probability that they originate from the same distribution. For both high and low CSC rate groups, the vast majority of resulting p-values exceed 0.10, meaning we cannot discount the possibility that both groups follow a Gutenberg-Richter distribution (Fig. S8).

In any case, the difference in MFD calculated at high and low CSC rate cannot be interpreted as a result of a different detection level. The shape of both distributions roll over similarly at low magnitudes, indicating a similar detection level.

5.3 Possible mechanisms behind b-value variation with Coulomb stress change rate

We find a positive correlation between b-value and CSC rate, but no significant correlation between b-value and CSC when seasonal variations are accounted. Our observations therefore seem to contradict the numerous studies which show the influence of stress on the MFD (T. Goebel et al., 2013; Scholz, 1968, 2015; Rivière et al., 2018; Tan et al., 2019; Dublanchet, 2022; Ito & Kaneko, 2023; Bourne & Oates, 2020; Gulia, 2023; Muntendam-Bos & Grobbe, 2022; Kraaijpoel et al., 2022; Mukuhira et al., 2024). The effect of stress on earthquake magnitude might not be visible in our study because the influence of CSC rate is dominant.

There is experimental evidence that stress rate can influence nucleation size, which in turn affects magnitude. Guérin-Marthe et al. (2019) showed that the critical nucleation length of laboratory earthquakes decreases approximately with the logarithm of shear stress rate. Numerical experiments by Dublanchet (2020) show that decreasing nucleation length likely inhibits earthquake growth, resulting in larger b-values. Assuming that increasing shear stress rate correlates with increasing CSC rate, our results may indicate a decrease of nucleation length with increasing shear stress rate. We caution, however, that this is merely speculation and that experiments involving both normal and shear stress rate are necessary before definitive conclusions can be drawn.

5.4 Implications for seismic hazard and magnitude forecast

We demonstrate that the MFD of induced earthquakes at Groningen varies in space, possibly in relation to the reservoir thickness. Because the b-value seems to increase with the CSC rate and plateaus, a conservative hypothesis for seismic hazard assessment would be to assume a b-value at the lower end of the distribution (0.6-0.8). The prospective forecast for the current plan to shut down production at Groningen by 2025 would, then, not be very different from the forecast obtained by Bourne and Oates (2020) based on the hypothesis of a correlation between annually averaged stress and the MFD. Since the CSC will remain high in the future while the CSC rate will decrease (because of the decision to shut down production), the two hypotheses would yield similar forecasts. They would, however, diverge if variations in CSC and CSC rates were not anti-correlated. In any case, the dependence of b-value on the CSC rate could be implemented in a stress-based seismicity forecast like Kaveh et al. (2023).

We note that the b-absolute and b-positive values are smaller than the values obtained with the other methods. This is probably because, to maximize the amount of data used, we assumed that magnitude differences as small as ($\sim$0.01) can be resolved. Assuming a resolution of 0.15 - 0.30 bumps up the b-absolute and b-positive values by 0.1, but the correlation between b-value and CSC rate remains the same. We therefore caution the reader against taking the b-positive and b-absolute values at face value. Using the b-value determined from the b-positive or b-absolute method would overestimate the hazard level at magnitudes higher than 2.

6 Conclusion

Earthquakes induced by gas extraction from the Groningen reservoir show systematic variations in b-value with space and Coulomb stress change rate. Spatial variations can be largely attributed to reservoir thickness, while the variation with stress change rate might be due to the effect of stress change rate on nucleation size. Whether the sensitivity of b-value to stress change rate applies to induced seismicity in general is unclear and probably worth further investigation.

Open Research Section

The data and codes necessary for this paper's analyses are available online at `https://doi.org/10.5281/zenodo.11111736`.

Acknowledgments

We thank Krittanon (Pond) Sirorattanakul, Hojjat Kaveh, Linxuan Li, Kyungjae (KJ) Im, Nicholas van der Elst, Thomas Goebel, and Bernard Dost for their help and comments. This study was supported by the NSF/Industry-University Collaborative Research Center 'Geomechanics and Mitigation of Geohazards' (National Science Foundation award No. 1822214) and the Enhancement Project GMG-3 funded by NAM. Y.T. acknowledges funding from the NSF Graduate Research Fellowship Program (National Science Foundation Grant No. 2139433). M.A. acknowledges funding from the Swiss National Science Foundation through Grant P2ELP2_195127.

References

Acosta, M., Avouac, J.-P., Smith, J. D., Sirorattanakul, K., Kaveh, H., & Bourne, S. J. (2023). Earthquake nucleation characteristics revealed by seismicity response to seasonal stress variations induced by gas production at Groningen. *Geophysical Research Letters*, *50*(19), e2023GL105455. doi: 10.1029/2023GL105455

Aki, K. (1965). Maximum likelihood estimate of b in the formula log N = a - bM and its confidence limits. *Bulletin of Earthquake Research*(43), 237–239.

Boitz, N., Langenbruch, C., & Shapiro, S. A. (2024). Production-induced seismicity indicates a low risk of strong earthquakes in the Groningen gas field. *Nature Communications*, *15*(1), 329. doi: 10.1038/s41467-023-44485-4

Bommer, J. J., & van Elk, J. (2017). Comment on "the maximum possible and the maximum expected earthquake magnitude for production-induced earthquakes at the gas field in Groningen, The Netherlands" by Gert Zöller and Matthias Holschneider. *Bulletin of the Seismological Society of America*, *107*(3), 1564–1567. doi: 10.1785/0120170040

Bourne, S. J., & Oates, S. J. (2017). Extreme threshold failures within a heterogeneous elastic thin sheet and the spatial-temporal development of induced seismicity within the Groningen gas field. *Journal of Geophysical Research: Solid Earth*, *122*(12), 10,299–10,320. doi: 10.1002/2017JB014356

Bourne, S. J., & Oates, S. J. (2020). Stress-dependent magnitudes of induced earthquakes in the Groningen gas field. *Journal of Geophysical Research: Solid Earth*, *125*(11), e2020JB020013. doi: 10.1029/2020JB020013

Bourne, S. J., Oates, S. J., & van Elk, J. (2018). The exponential rise of induced seismicity with increasing stress levels in the Groningen gas field and its implications for controlling seismic risk. *Geophysical Journal International*, *213*(3), 1693–1700. doi: 10.1093/gji/ggy084

Bourne, S. J., Oates, S. J., van Elk, J., & Doornhof, D. (2014). A seismological model for earthquakes induced by fluid extraction from a subsurface reservoir. *Journal of Geophysical Research: Solid Earth*, *119*(12), 8991–9015. doi: 10.1002/2014JB011663

Candela, T., Osinga, S., Ampuero, J.-P., Wassing, B., Pluymaekers, M., Fokker, P. A., ... Muntendam-Bos, A. G. (2019). Depletion-induced seismicity at the Groningen gas field: Coulomb rate-and-state models including differential compaction effect. *Journal of Geophysical Research: Solid Earth*, *124*(7), 7081–7104. doi: 10.1029/2018JB016670

de Jager, J., & Visser, C. (2017). Geology of the Groningen field – an overview. *Netherlands Journal of Geosciences*, *96*(5), s3–s15. doi: 10.1017/njg.2017.22

Dempsey, D. E., & Suckale, J. (2023). Physics-based forecasting of induced seismicity at Groningen gas field, the Netherlands: Post hoc evaluation and forecast update. *Seismological Research Letters*, *94*(3), 1429–1446. doi: 10.1785/0220220317

Dost, B., Ruigrok, E., & Spetzler, J. (2017). Development of seismicity and probabilistic hazard assessment for the Groningen gas field. *Netherlands Journal of Geosciences*, *96*(5), s235–s245. doi: 10.1017/njg.2017.20

Dublanchet, P. (2020). Stress-dependent b value variations in a heterogeneous rate-and-state fault model. *Geophysical Research Letters*, *47*(13). doi: 10 .1029/2020GL087434

Dublanchet, P. (2022). Shear stress and b-value fluctuations in a hierarchical rate-and-state asperity model. *Pure and Applied Geophysics*, *179*(6-7), 2423–2435. doi: 10.1007/s00024-022-03039-3

Goebel, T., Schorlemmer, D., Becker, T. W., Dresen, G., & Sammis, C. G. (2013). Acoustic emissions document stress changes over many seismic cycles in stick-slip experiments. *Geophysical Research Letters*, *40*(10), 2049–2054. doi: 10.1002/grl.50507

Goebel, T. H., Kwiatek, G., Becker, T. W., Brodsky, E. E., & Dresen, G. (2017). What allows seismic events to grow big?: Insights from b-value and fault roughness analysis in laboratory stick-slip experiments. *Geology*, *45*(9), 815–818. doi: 10.1130/G39147.1

Guérin-Marthe, S., Nielsen, S., Bird, R., Giani, S., & Di Toro, G. (2019). Earthquake nucleation size: Evidence of loading rate dependence in laboratory faults. *Journal of Geophysical Research: Solid Earth*, *124*(1), 689–708. doi: 10.1029/2018JB016803

Gulia, L. (2023). Time–space evolution of the Groningen gas field in terms of *b* -value: Insights and implications for seismic hazard. *Seismological Research Letters*. doi: 10.1785/0220220396

Gutenberg, B., & Richter, C. F. (1944). Frequency of earthquakes in California. *Bulletin of the Seismological Society of America*, *34*(4), 185–188. doi: 10.1785/BSSA0340040185

Ito, R., & Kaneko, Y. (2023). Physical mechanism for a temporal decrease of the Gutenberg-Richter b-Value prior to a large earthquake. *Journal of Geophysical Research: Solid Earth*, *128*(12), e2023JB027413. doi: 10.1029/2023JB027413

Kaveh, H., Batlle, P., Acosta, M., Kulkarni, P., Bourne, S. J., & Avouac, J. P. (2023). Induced seismicity forecasting with uncertainty quantification: Application to the Groningen gas field. *Seismological Research Letters*, *95*(2A), 773–790. doi: 10.1785/0220230179

Kijko, A., & Smit, A. (2012). Extension of the Aki-Utsu b-value estimator for incomplete catalogs. *Bulletin of the Seismological Society of America*, *102*, 1283–1287. doi: 10.1785/0120110226

KNMI. (2023). Earthquakes - complete catalogue for the Netherlands and near surrounding. Retrieved from `https://dataplatform.knmi.nl/dataset/aardbevingen-catalogus-1`

Kraaijpoel, D., Martins, J. E., Osinga, S., Vogelaar, B., & Breunese, J. (2022). Statistical analysis of static and dynamic predictors for seismic b-value variations in the Groningen gas field. *Netherlands Journal of Geosciences*, *101*, e18. doi: 10.1017/njg.2022.15

Li, L., Luo, G., & Liu, M. (2023). The K-M slope: a potential supplement for b-value. *Seismological Research Letters*, *94*(4), 1892–1899. doi: 10.1785/0220220268

Meyer, H., Smith, J. D., Bourne, S., & Avouac, J.-P. (2023). An integrated framework for surface deformation modelling and induced seismicity forecasting due to reservoir operations. *Geological Society, London, Special Publications*, *528*(1), SP528–2022–169. doi: 10.1144/SP528-2022-169

Mukuhira, Y., Fehler, M. C., Bjarkason, E. K., Ito, T., & Asanuma, H. (2024). On the *b*-value dependency of injection-induced seismicity on geomechanical parameters. *International Journal of Rock Mechanics and Mining Sciences*, *174*, 105631. doi: 10.1016/j.ijrmms.2023.105631

Mukuhira, Y., Fehler, M. C., Ito, T., Asanuma, H., & Häring, M. O. (2021). Injection-induced seismicity size distribution dependent on shear stress. *Geophysical Research Letters*, *48*(8), e2020GL090934. doi: 10.1029/2020GL090934

Muntendam-Bos, A. G., & Grobbe, N. (2022). Data-driven spatiotemporal assessment of the event-size distribution of the Groningen extraction-induced seismicity catalogue. *Scientific Reports*, *12*(1), 10119. doi: 10.1038/s41598-022-14451-z

Oates, S., Landman, A. J., van der Wal, O., Baehr, H., & Piening, H. (2022). Geomechanical, seismological, and geodetic data pertaining to the groningen gas field: a data package used in the "mmax ii workshop", on constraining the maximum earthquake magnitude in the groningen field (version 1.0) [data set]. *Utrecht University, https://doi.org/10.24416/UU01-RHHRPY*.

Richter, G., Hainzl, S., Dahm, T., & Zöller, G. (2020). Stress-based, statistical modeling of the induced seismicity at the Groningen gas field, The Netherlands. *Environmental Earth Sciences*, *79*(11), 252. doi: 10.1007/s12665-020-08941-4

Rivière, J., Lv, Z., Johnson, P. A., & Marone, C. (2018). Evolution of b-value during the seismic cycle: Insights from laboratory experiments on simulated faults. *Earth and Planetary Science Letters*, *482*, 407–413. doi: 10.1016/j.epsl.2017.11.036

Scholz, C. (1968). The frequency-magnitude relation of microfracturing in rock and its relation to earthquakes. *Bulletin of the Seismological Society of America*, *58*(1), 399–415. doi: 10.1785/BSSA0580010399

Scholz, C. (2015). On the stress dependence of the earthquake b value. *Geophysical Research Letters*, *42*(5), 1399–1402. doi: 10.1002/2014GL062863

Schorlemmer, D., Wiemer, S., & Wyss, M. (2005). Variations in earthquake-size distribution across different stress regimes. *Nature*, *437*(7058), 539–542. doi: 10.1038/nature04094

Smith, J. D., Heimisson, E. R., Bourne, S. J., & Avouac, J.-P. (2022). Stress-based forecasting of induced seismicity with instantaneous earthquake failure functions: Applications to the Groningen gas reservoir. *Earth and Planetary Science Letters*, *594*, 117697. doi: 10.1016/j.epsl.2022.117697

Smith, J. D., White, R. S., Avouac, J.-P., & Bourne, S. (2020). Probabilistic earthquake locations of induced seismicity in the Groningen region, the Netherlands. *Geophysical Journal International*, *222*(1), 507–516. doi: 10.1093/gji/ggaa179

Stirling, M. W., Wesnousky, S. G., & Shimazaki, K. (1996). Fault trace complexity, cumulative slip, and the shape of the magnitude-frequency distribution for strike-slip faults: a global survey. *Geophysical Journal International*, *124*(3), 833–868. doi: 10.1111/j.1365-246X.1996.tb05641.x

Tan, Y. J., Waldhauser, F., Tolstoy, M., & Wilcock, W. S. (2019). Axial Seamount: Periodic tidal loading reveals stress dependence of the earthquake size distribution (b value). *Earth and Planetary Science Letters*, *512*, 39–45. doi: 10.1016/j.epsl.2019.01.047

van der Elst, N. J. (2021). B-positive: a robust estimator of aftershock magnitude distribution in transiently incomplete catalogs. *Journal of Geophysical Research: Solid Earth*, *126*(2), e2020JB021027. doi: 10.1029/2020JB021027

Zöller, G., & Holschneider, M. (2016). The maximum possible and the maximum expected earthquake magnitude for production-induced earthquakes at the gas field in Groningen, The Netherlands. *Bulletin of the Seismological Society of America*, *106*(6), 2917–2921. doi: 10.1785/0120160220

Zöller, G., & Hainzl, S. (2022). Seismicity Scenarios for the Remaining Operating Period of the Gas Field in Groningen, Netherlands. *Seismological Research Letters*, *94*(2A), 805–812. doi: 10.1785/0220220308

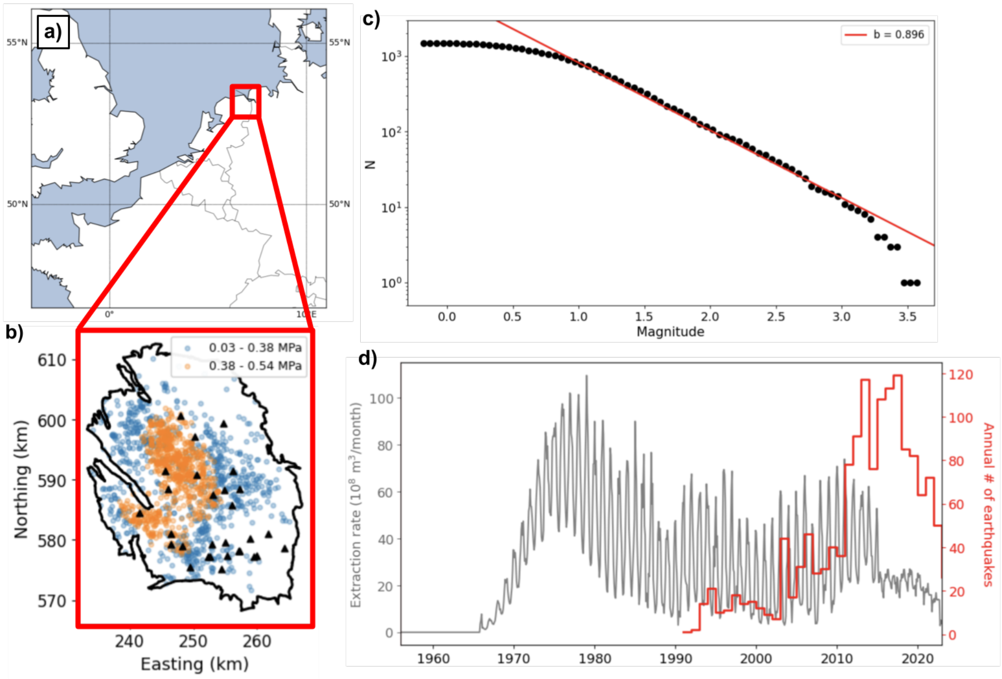

Figure 1. (a) Setting of Groningen reservoir. (b) Reservoir outline with earthquakes between December 1991 and July 2023. High CSC earthquakes are plotted in orange and low CSC earthquakes are plotted in blue. For consistency with Bourne and Oates (2020), stresses are annually averaged. Triangles show well locations. (c) MFD; red line corresponds to a b-value of 0.896. (d) Time-series showing monthly rate of gas extraction (grey) and annual number of earthquakes (red).

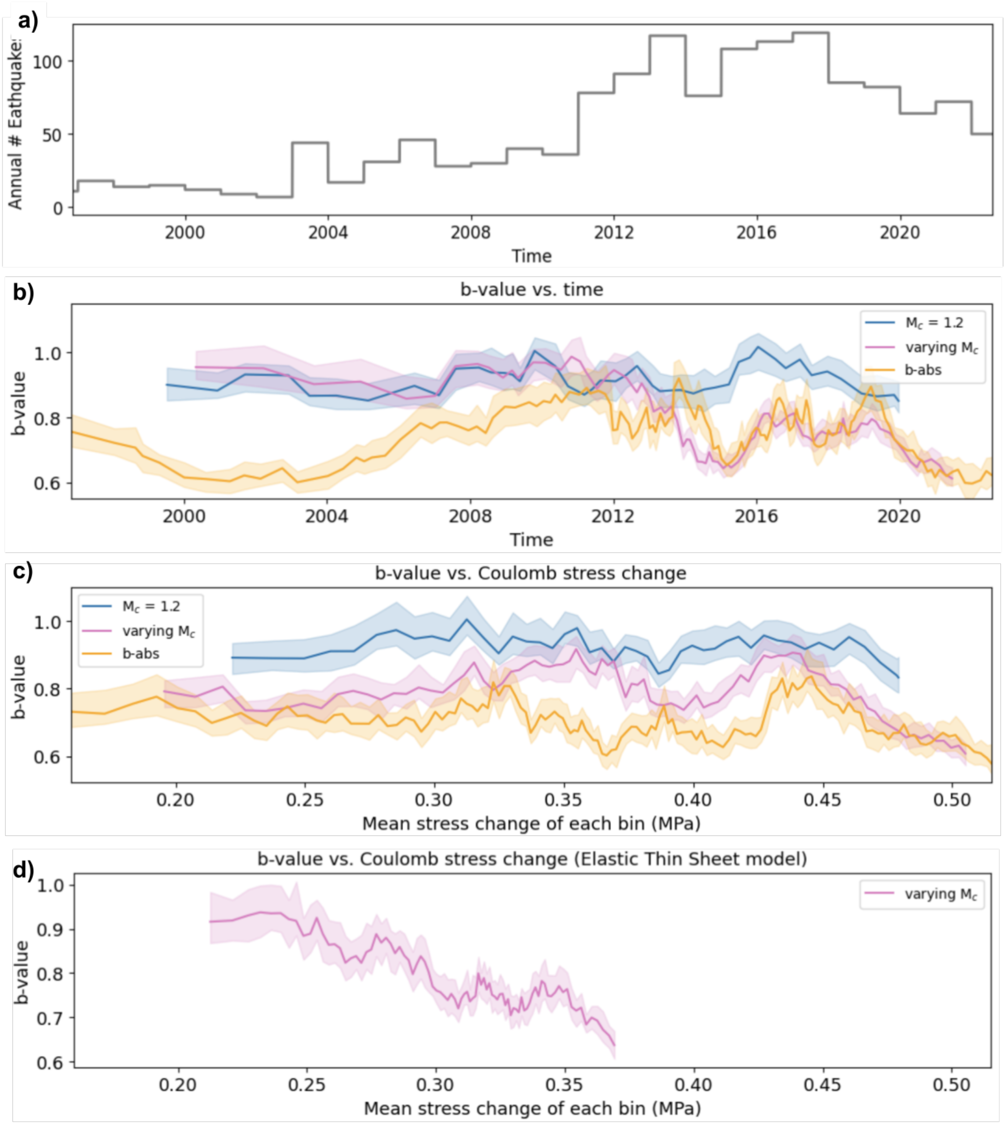

Figure 2. (a) Time series of the number of earthquakes per year. (b) Variation of b-value with time. Variation of b-value with CSC using the (c) reference model and (d) Elastic Thin Sheet model. b-values are calculated using maximum likelihood (blue), modified maximum likelihood with varying M_C (pink), and b-absolute methods (orange). Shaded regions represent the 16th through 84th percentiles of each bin. Note that the b-absolute method yields b-values at extreme values of time and stress, as the lack of limitation by catalog incompleteness allows the use of more data.

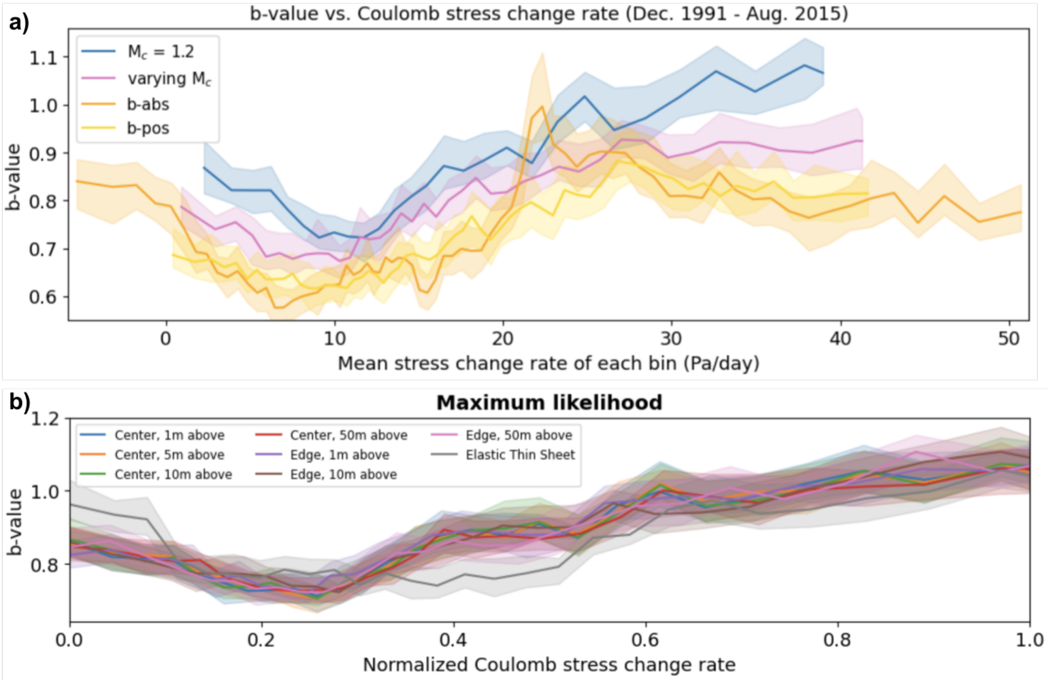

Figure 3. (a) Variation of b-value with CSC rate. b-values are calculated using maximum likelihood (blue), modified maximum likelihood with varying M_C (pink), b-absolute (orange), and b-positive (yellow) methods. CSC rates are calculated using the reference model. Note that the b-absolute method yields b-values at extreme values of CSC rate, as the lack of limitation by catalog incompleteness allows us to use more data. (b) Variation of b-value, calculated using maximum likelihood method (Aki, 1965). CSC rates are calculated using different sampling schemes of the mechanical model and the Elastic Thin Sheet model (Bourne & Oates, 2017) (Table S1), and normalized to a scale of 0 to 1. Shaded regions represent the 16th through 84th percentiles of each bin.

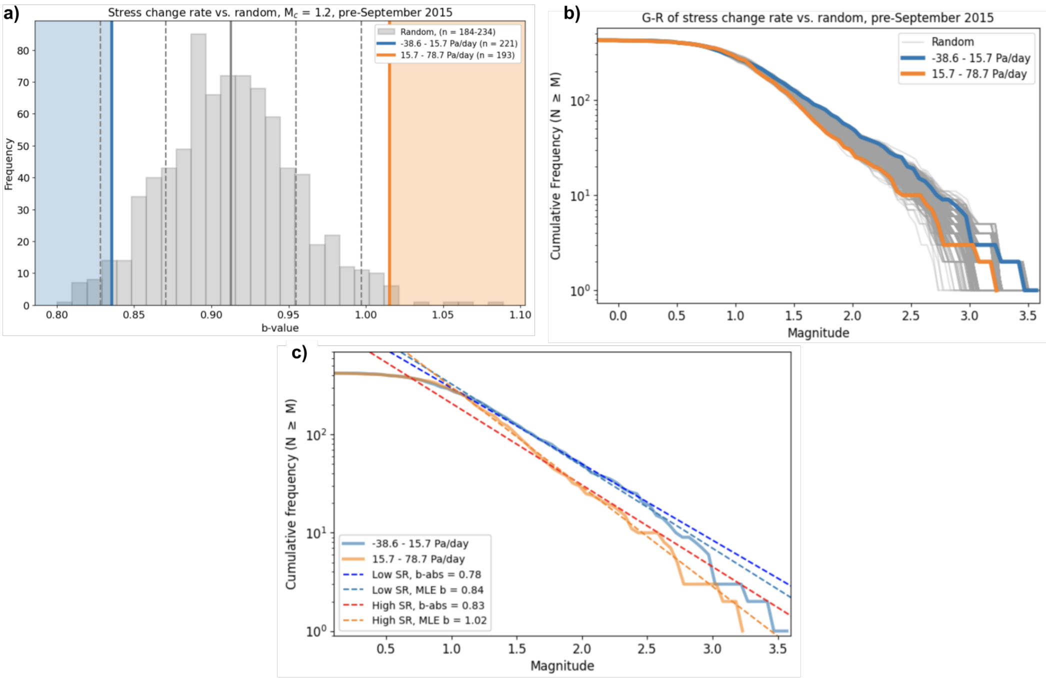

Figure 4. (a) Histogram of b-values for 800 randomly-generated samples (grey), alongside b-values calculated when splitting the catalog into high (blue line) and low (orange line) CSC rate. CSC rates are calculated using the reference model. Solid grey line shows mean b-value of random samples, and dotted grey lines show 1-2 standard deviations from the mean. All b-values are calculated using the maximum likelihood method. (b) MFD of randomly-selected samples (grey), low CSC rate group (blue), and high CSC rate group (orange). (c) MFD of earthquake catalog, split into high (solid orange line) and low (solid blue line) CSC rate. Dotted dark blue and red lines plot b-absolute values at low and high CSC rate. Dotted blue and orange lines plot maximum likelihood b-values at low and high CSC rate.